



Perpendicular magnetic anisotropy induced by NiMn-based antiferromagnetic films with in-plane spin orientations: Roles of interfacial and volume antiferromagnetic moments

Bo-Yao Wang ^{1,*}, Chung-Hsuan Hsiao ¹, Bo-Xiang Liao,¹ Chun-Yao Hsu,¹ Tzu-Hsin Li,¹ Yen-Ling Hsu,¹ Yen-Ming Lai,¹ Ming-Shian Tsai,^{1,2} Tzu-Hung Chuang,³ and Der-Hsin Wei³

¹*Department of Physics, National Changhua University of Education, Changhua 500, Taiwan*

²*Institute of Photonics Technologies, National Tsing Hua University, Hsinchu 300, Taiwan*

³*National Synchrotron Radiation Research Center, Hsinchu 300, Taiwan*



(Received 20 May 2021; revised 28 June 2021; accepted 8 July 2021; published 19 July 2021)

Antiferromagnetic (AFM) thin films are promising materials for engineering the magnetic anisotropy of adjacent ferromagnetic (FM) films. In this work, we explored the effects of triggering perpendicular magnetic anisotropy (PMA) of FM films by applying a series of NiMn-based AFM films with in-plane-oriented spin structures. The vertically expanded face-centered tetragonal $\text{Ni}_{50}\text{Mn}_{50}$ films alone could not induce PMA in Co/Ni films. By contrast, PMA was triggered through the application of Mn-rich NiMn alloy films or $\text{Ni}_{50}\text{Mn}_{50}/1\text{-monolayer Mn}$ (Mn/1-ML $\text{Ni}_{50}\text{Mn}_{50}$) heterostructures. Detailed analyses of a series of samples indicated that two criteria must be met for a NiMn-based AFM film to trigger PMA in a neighboring FM film: (1) perpendicular interface crystalline anisotropy of interfacial uncompensated Mn moments must be established, and (2) strengthened lateral exchange coupling to volume AFM moments must be made. This paper clarifies how NiMn-based AFM films with in-plane-oriented AFM spin structures trigger the PMA of FM films, thus identifying a pathway to increase control over antiferromagnet-induced PMA through the interface/volume magnetic engineering of AFM layers.

DOI: [10.1103/PhysRevB.104.024424](https://doi.org/10.1103/PhysRevB.104.024424)

I. INTRODUCTION

Antiferromagnetic (AFM) thin films with compelling physical properties and myriad potential applications have attracted considerable scholarly interest in the field of magnetism. Upon placement next to a ferromagnet [1–4], the effects of induced coercivity (H_c) enhancement and exchange bias can be applied in the design of magnetic logic devices such as spin valves to stabilize the magnetization of a magnetic reference layer during the magnetization switching of a magnetic storage layer [5]. Recently, reports have suggested that an AFM film can also trigger perpendicular magnetization in ferromagnetic (FM) layers [6–9]. With the advantage of being able to flexibly control perpendicular H_c and full magnetization [6,8], this approach has the potential to become an alternative method for ameliorating the control of perpendicular magnetic anisotropy (PMA) in future spintronic devices. According to the literature, the PMA triggered by AFM films exhibits varying behavior that is determined by the spin structure and interface condition of the AFM film. For instance, fcc- $\text{Fe}_{50}\text{Mn}_{50}$ films with a three-dimensional quadratic-type spin structure [10–13] can induce robust PMA in adjacent Co/Ni films [8]. Moreover, PMA can also be triggered by vertically expanded face-centered tetragonal (e-fct) Mn films [9] that exhibit a two-dimensional layered AFM spin structure [14,15]. However, to date, only a few AFM/FM systems have been demonstrated to exhibit antiferromagnet-induced PMA. To extend the knowledge of this phenomenon and facilitate

the development of potential applications for perpendicularly magnetic devices, exploring the effects of antiferromagnet-induced PMA on other AFM/FM systems is crucial.

Among Mn-based AFM alloys, NiMn has attracted special interest because of its high thermal stability, corrosion resistance, and high Néel temperature (1070 K) [16–18]. Bulk $\text{Ni}_{50}\text{Mn}_{50}$ exhibits an L_{10} -type vertically contracted face-centered tetragonal (c-fct) structure with lattice constants $a = b = 3.74 \text{ \AA}$ and $c = 3.52 \text{ \AA}$ [19], whereas Mn and Ni atoms occupy alternating atomic sheets perpendicular to the c axis. When grown on Cu(001) or Co/Cu(001), $\text{Ni}_{50}\text{Mn}_{50}$ films exhibit an e-fct or a -axis-grown structure with lattice constants $a = b = 3.61 \text{ \AA}$ and $c = 3.75 \text{ \AA}$ [20,21]. In this configuration, the Ni and Mn atomic sheets are oriented perpendicular to the Cu(001) surface, forming a $c(2 \times 2)$ -ordered atomic structure in each layer. According to a spin-polarized scanning tunneling microscopy (SP-STM) study on e-fct $\text{Ni}_{50}\text{Mn}_{50}$ films [22], Ni and Mn exhibit nearly opposite in-plane spin polarization at a chemically ordered equiatomic NiMn(001) surface, although a noncollinear in-plane spin configuration could arise from a $p(2 \times 2)$ surface reconstruction in association with the upward (downward) relaxation of Mn (Ni) surface atoms. The SP-STM study also indicated that the surface magnetic moment density of Mn (3.69 or 3.91 μ_B/atom) is considerably higher than the value of Ni (0.08 or 0.3 μ_B/atom) [22]. Hence, the contribution of AFM-induced coupling in those $\text{Ni}_{50}\text{Mn}_{50}$ /FM exchange-coupled systems is expected to be mainly attributable to Mn moments. Because of similar in-plane spin orientations but differing Mn moment density between the $\text{Ni}_{50}\text{Mn}_{50}$ and Mn films [14,15,22], as displayed in Fig. 1, NiMn-based AFM/FM films could be designed as

*bywang1735@cc.ncue.edu.tw

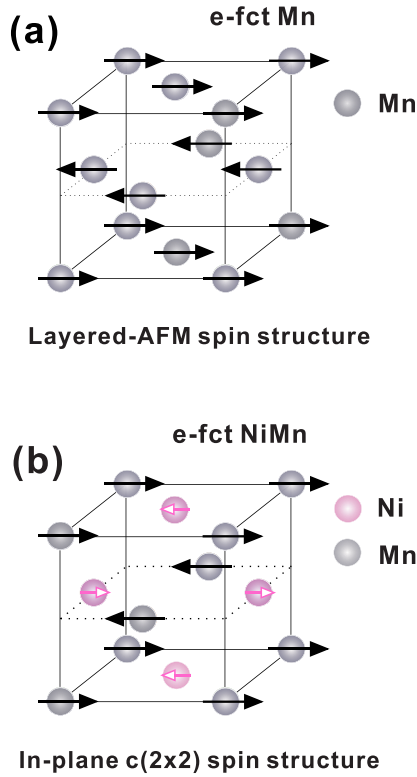


FIG. 1. (a) and (b): schematic illustrations of the layered AFM and in-plane $c(2 \times 2)$ spin structures of the e-fct Mn and e-fct (or a -axis-grown) $\text{Ni}_{50}\text{Mn}_{50}$ films, respectively, according to the literature [14,15,22].

model systems for exploring the effects of PMA triggered by AFM films with in-plane-oriented spin structures, the mechanism of which remains unclear.

In this study, we investigated the effects of triggering the PMA of FM films through the application of a series of NiMn-based AFM films with in-plane-oriented spin structures. We demonstrated that e-fct $\text{Ni}_{50}\text{Mn}_{50}$ films alone cannot induce Co/Ni film PMA at room temperature; however, PMA can be induced by applying Mn-rich NiMn alloy films or $\text{Ni}_{50}\text{Mn}_{50}/1\text{-ML Mn}$ ($\text{Mn}/1\text{-ML Ni}_{50}\text{Mn}_{50}$) heterostructures. Our detailed analysis indicated that two criteria are essential for a NiMn-based AFM film to trigger PMA in a neighboring FM film: (1) perpendicular interface crystalline anisotropy of the interfacial uncompensated Mn moments must be established, and (2) a strengthened lateral exchange coupling to the volume AFM moments must be made. Our study clarifies the mechanism that triggers PMA via NiMn-based AFM films with an in-plane-oriented AFM spin structure, thus opening a pathway to increase control over antiferromagnet-induced PMA through the interface/volume magnetic engineering of AFM layers.

II. EXPERIMENT

In this study, the growth condition, crystalline structure, and magnetic properties of a series of NiMn-based AFM/FM films were investigated *in situ* in a multifunctional ultrahigh-vacuum chamber with a base pressure of 2×10^{-10} torr. Single crystalline Cu(001) substrates with a well-ordered crys-

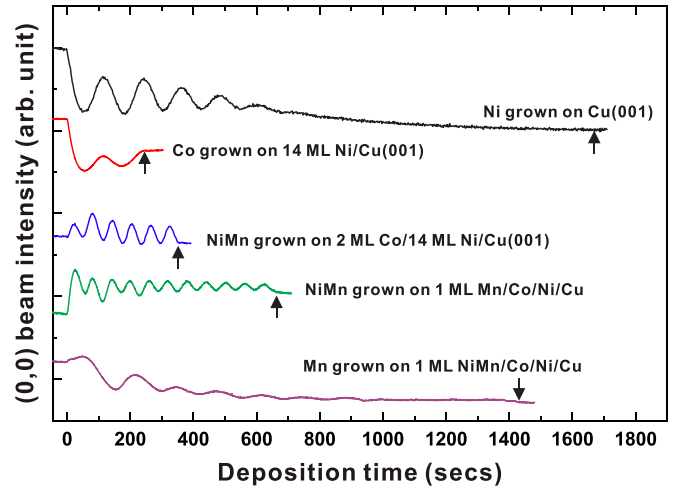


FIG. 2. Selected MEED (0,0) beam intensity curves as a function of deposition time for Ni film grown on Cu(001), Co film grown on 14-ML Ni/Cu(001), $\text{Ni}_{50}\text{Mn}_{50}$ film grown on 2-ML Co/14-ML Ni/Cu(001) (Co/Ni/Cu), $\text{Ni}_{50}\text{Mn}_{50}$ film grown on 1-ML Mn/Co/Ni/Cu, and Mn film grown on 1-ML $\text{Ni}_{50}\text{Mn}_{50}/\text{Co}/\text{Ni}/\text{Cu}$ at 300 K. Film thickness and deposition rate were calibrated by the oscillations in the MEED curves. The arrows indicate the time at which the shutter was closed.

talline structure and smooth surfaces were prepared through cycles of 2-keV Ar^+ ion sputtering and subsequent annealing at 800 K for 5 min. A series of NiMn-based AFM films, namely $\text{Ni}_{50}\text{Mn}_{50}$, $\text{Ni}_{40}\text{Mn}_{60}$, $\text{Ni}_{50}\text{Mn}_{50}/1\text{-ML Mn}$, and $\text{Mn}/1\text{-ML Ni}_{50}\text{Mn}_{50}$ films grown on 2-ML Co/14-ML Ni/Cu(001) (Co/Ni/Cu), were prepared at room temperature using electron gun (e -beam evaporator) with a flux monitor. During film growth, the deposition rate and thickness of the films were monitored through medium-energy electron diffraction (MEED). Figure 2 presents the typical specular MEED (0,0) beam intensity of the Ni film grown on Cu(001), Co films grown on 14-ML Ni/Cu(001), $\text{Ni}_{50}\text{Mn}_{50}$ grown on 0-, 1-ML Mn/Co/Ni/Cu, and Mn grown on 1-ML $\text{Ni}_{50}\text{Mn}_{50}/\text{Co}/\text{Ni}/\text{Cu}$. In general, regular oscillation indicates layer-by-layer growth conditions for these films. After a 14-ML Ni film was deposited on Cu(001), the sample was annealed at 430 K for 10 min to improve surface smoothness [23]. The alloy composition of the NiMn films was controlled by adjusting the individual deposition rates and was confirmed by Auger electron spectroscopy. The in-plane film structure was probed by applying low-energy electron diffraction (LEED). The average vertical interlayer distances of the films were measured using LEED I/V with a kinematic approximation [24]. The magnetic hysteresis loops of the samples were measured *in situ* through magneto-optic Kerr effects (MOKE) in both longitudinal and polar geometries at room temperature. The magnetic properties of the individual elements in perpendicularly magnetic NiMn-based AFM/Co/Ni films were detected by assessing the x-ray magnetic circular dichroism (XMCD) effects [25] measured at the Mn, Co, and Ni $L_{3,2}$ absorption edges in total electron yield mode. These measurements were performed in an x-ray photoemission electron microscopy (PEEM) [26–28] end station at Beamline BL05B2 of the National Synchrotron Radiation Research

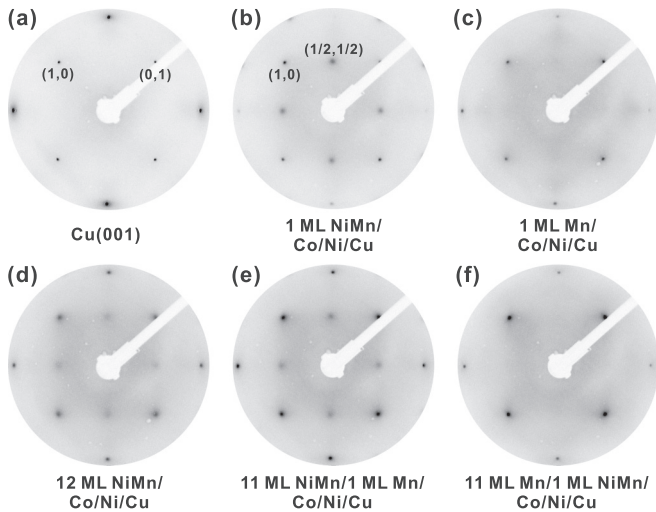


FIG. 3. LEED patterns of (a) Cu(001), (b) 1-ML Ni₅₀Mn₅₀/Co/Ni/Cu, (c) 1-ML Mn/Co/Ni/Cu, (d) 12-ML Ni₅₀Mn₅₀/Co/Ni/Cu, (e) 11-ML Ni₅₀Mn₅₀/1-ML Mn/Co/Ni/Cu, and (f) 11-ML Mn/1-ML Ni₅₀Mn₅₀/Co/Ni/Cu. The measurements were performed at 110 eV and 300 K.

Center in Hsinchu, Taiwan. The x-ray absorption spectra (XAS) are normalized by the incident beam intensity as well as the edge jump of L_{3,2}. Because of a full-magnetic-shielding

design in this PEEM end station, the measurements of the XAS and XMCD curves were under remanent conditions. The remnant magnetic states of the sample were generated by applying either a positive or negative external magnetic field (± 1000 Oe) along the out-of-plane direction before placing it in the PEEM sample holder.

III. RESULTS

A. Crystalline structure of Ni₅₀Mn₅₀-based AFM films grown on 2-ML Co/14-ML Ni/Cu(001)

Figures 3(a)–3(f) display selected LEED patterns of Cu(001) and 1-ML Ni₅₀Mn₅₀, 1-ML Mn, 12-ML Ni₅₀Mn₅₀, 11-ML Ni₅₀Mn₅₀/1-ML Mn, and 11-ML Mn/1-ML Ni₅₀Mn₅₀ films grown on Co/Ni/Cu; these patterns were measured at 110 eV. We observed that the $p(1 \times 1)$ spots of these films were located at the same positions as those of Cu(001), indicating an epitaxial growth condition. Therefore, the in-plane lattice constants (a_{\parallel}) of those Ni₅₀Mn₅₀ or Mn films were determined to equal 3.61 Å [lattice constant of Cu(001)]. Moreover, a clear $c(2 \times 2)$ structure was observed in the 1-ML Ni₅₀Mn₅₀/Co/Ni, 12-ML Ni₅₀Mn₅₀/Co/Ni, and 11-ML Ni₅₀Mn₅₀/1-ML Mn/Co/Ni films. This indicates the formation of a chemically ordered equiatomic structure on the top surface of the grown Ni₅₀Mn₅₀ films, which matches

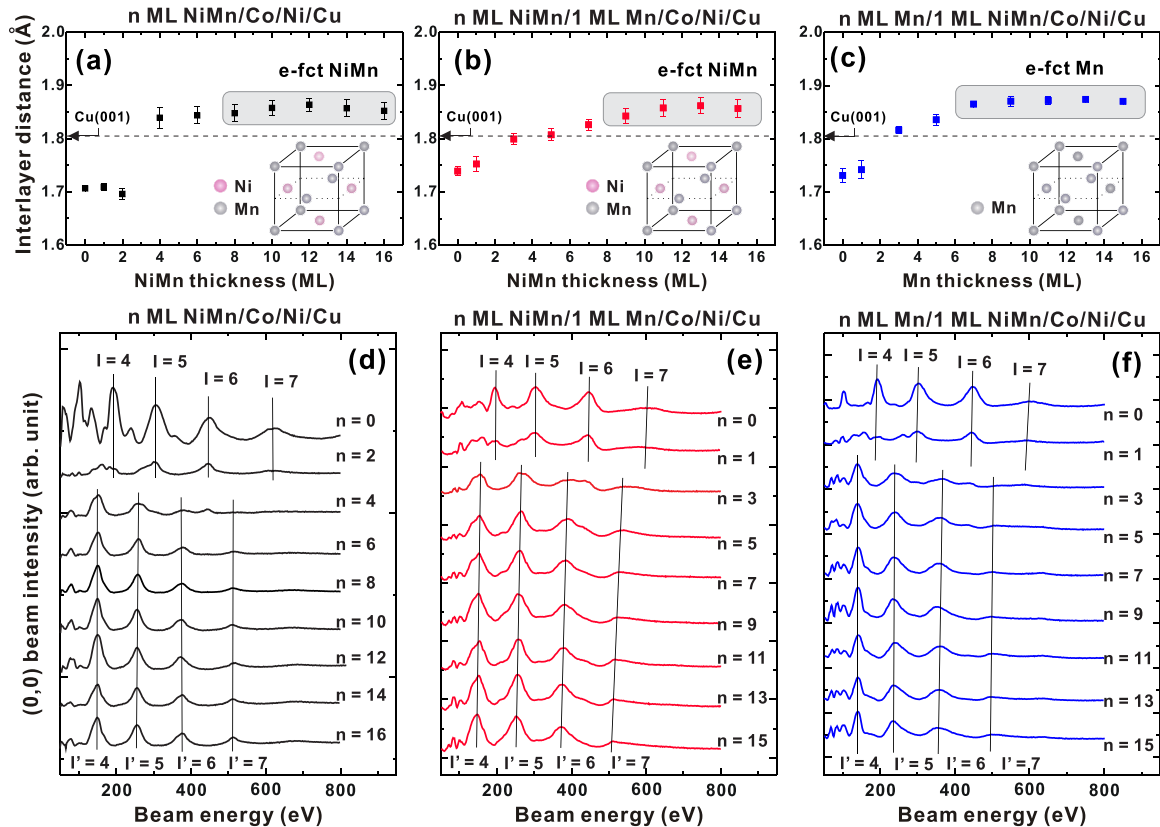


FIG. 4. Average interlayer distance d_{\perp} of (a) 0–16-ML Ni₅₀Mn₅₀ films grown on Co/Ni/Cu, (b) 0–15-ML Ni₅₀Mn₅₀ films grown on 1-ML Mn/Co/Ni/Cu, and (c) 0–15-ML Mn films grown on 1-ML Ni₅₀Mn₅₀/Co/Ni/Cu, as calculated according to the energy peaks (I or I') of the corresponding LEED specular spot I/V curves of (d), (e), and (f), respectively, measured at 300 K. In (a)–(c), the dashed lines represent the d_{\perp} of Cu(001). The shadows indicate the formation of stable e-fct Ni₅₀Mn₅₀ or e-fct Mn films. The illustrations in insets display the schematic atomic structure of e-fct Ni₅₀Mn₅₀ or e-fct Mn films.

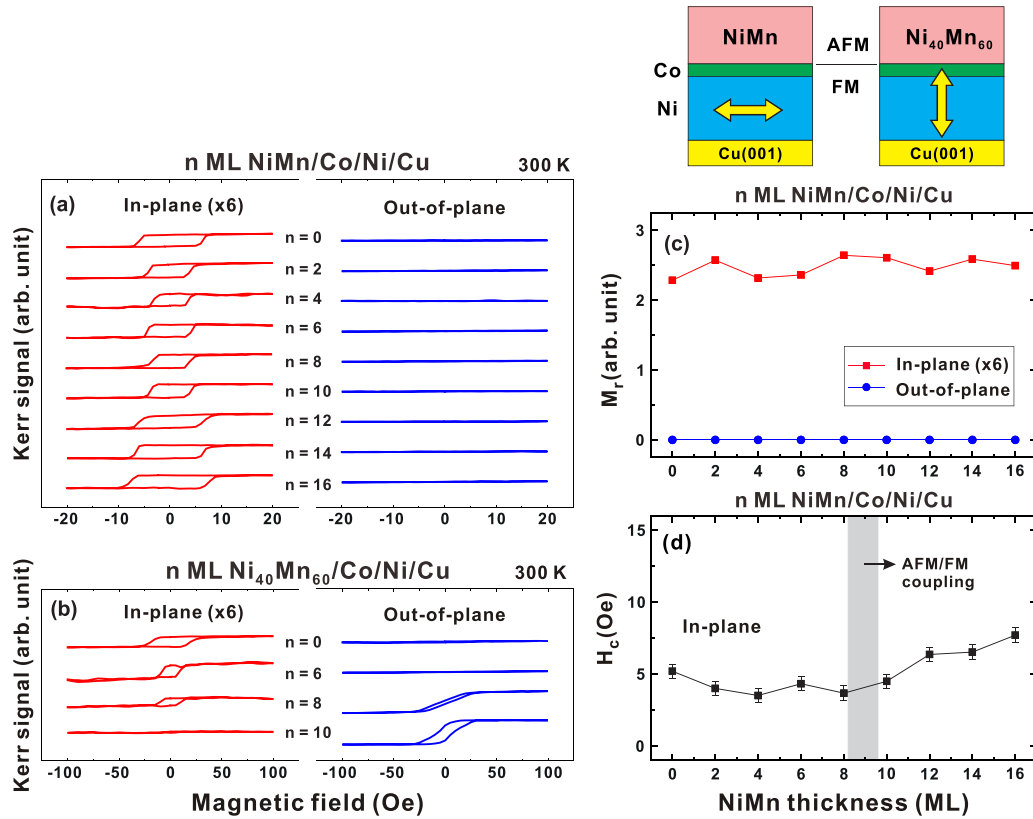


FIG. 5. Magnetic hysteresis loops of (a) 0–16-ML Ni₅₀Mn₅₀/Co/Ni/Cu and (b) 0–10-ML Ni₄₀Mn₆₀/Co/Ni/Cu. The measurements were performed at room temperature. (c) and (d): summarized M_r and H_c values of 0–16-ML Ni₅₀Mn₅₀/Co/Ni/Cu according to the magnetic hysteresis loops of (a). In (d), the gray shadow indicates the estimated critical thickness for the onset of AFM–FM exchange coupling (H_c enhancement) as well as an established long-range AFM ordering of Ni₅₀Mn₅₀ films at room temperature.

the surface structure of Ni₅₀Mn₅₀ films grown on Cu(001) or Co/Cu(001) [20,21].

Figures 4(a)–4(c) present the average interlayer distance (d_{\perp}) values of various Ni₅₀Mn₅₀ films grown on 0-, 1-ML Mn/Co/Ni/Cu and Mn films grown on 1-ML Ni₅₀Mn₅₀/Co/Ni/Cu, which were calculated according to the LEED I/V curves obtained from LEED specular spots [Figs. 4(d)–4(f)]. As shown in Figs. 4(a) and 4(b), the d_{\perp} values of all Ni₅₀Mn₅₀ films stabilized at approximately 1.86 Å when the thickness of Ni₅₀Mn₅₀ (t_{NiMn}) exceeded 8 ML; the Ni₅₀Mn₅₀ film exhibited a stable e-fct structure ($c/a \approx 1.03$), which is similar to the behavior of Ni₅₀Mn₅₀ films grown on Co/Cu(001) or Cu(001) [20,21]. In addition, the d_{\perp} values of Mn films grown on 1-ML Ni₅₀Mn₅₀/Co/Ni/Cu stabilized at 1.88 Å when the thickness of Mn (t_{Mn}) exceeded 5 ML; this also indicated the formation of a Mn film with a stable e-fct phase, and such behavior is similar to that of Mn films grown on Co/Ni/Cu [9].

B. Magnetic properties of Ni₅₀Mn₅₀/Co/Ni films

Figure 5(a) presents the magnetic hysteresis loops of the Ni₅₀Mn₅₀/Co/Ni films, which indicate in-plane magnetic anisotropy in the Co/Ni film. No distinguishable PMA was observed in Ni₅₀Mn₅₀/Co/Ni films although t_{NiMn} reached 16 ML. To examine the AFM properties of the prepared Ni₅₀Mn₅₀ films, determining the onset of long-range AFM

ordering was essential. In multiple previous studies [29–33], x-ray magnetic linear dichroism (XMLD) was adopted as a direct approach for examining the long-range AFM order of AFM films. However, acquiring distinguishable XMLD spectra for the present metallic AFM films was restricted by the design of a fixed orientation between the x-ray and sample holder and a full magnetic shielding in the sample holder of the PEEM setup. Thus, in the present work, the characteristic phenomenon of enhanced H_c engendered in AFM/FM systems was employed as a fingerprint to indicate the presence of long-range AFM ordering in our samples due to that approach having been justified in previous studies [3,34–37]. The examination of Ni₅₀Mn₅₀/Co/Ni films demonstrated that the H_c value was slightly enhanced when t_{NiMn} exceeded 8 ML [Fig. 5(d)], which is indicative of a threshold thickness of approximately 9 ML for the established long-range AFM ordering of the Ni₅₀Mn₅₀ films at room temperature. This threshold value and a finding of weak AFM coupling behaviors induced by Ni₅₀Mn₅₀ films are consistent with the results of previous reports [20,21]. Our results indicated that Ni₅₀Mn₅₀ films alone cannot induce PMA in adjacent Co/Ni films. However, when the Mn concentration was slightly increased to 60% [Fig. 5(b)] and t_{NiMn} exceeded 8 ML, weak PMA developed. This finding indicates that increasing Mn moment density in full NiMn films can promote the effects of induced PMA in adjacent Co/Ni films.

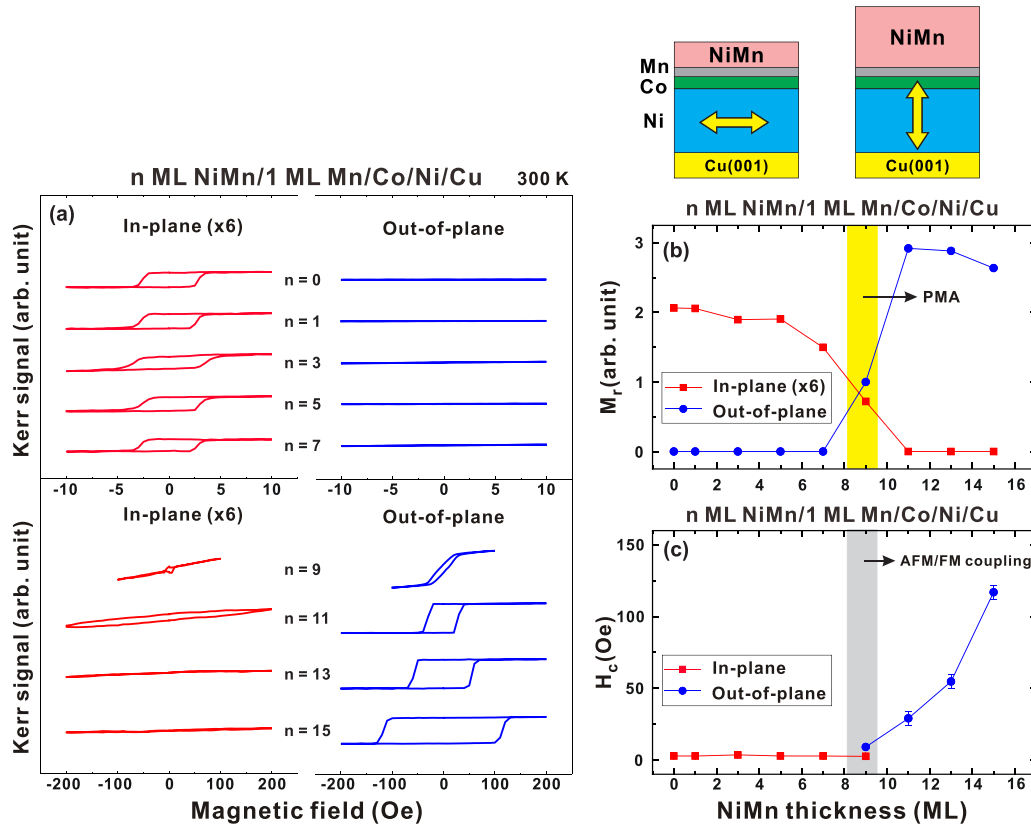


FIG. 6. Magnetic hysteresis loops of (a) 0–15-ML $\text{Ni}_{50}\text{Mn}_{50}/1\text{-ML Mn/Co/Ni/Cu}$. The measurements were performed at room temperature. (b) and (c): summarized M_r and H_c values of 0–15-ML $\text{Ni}_{50}\text{Mn}_{50}/1\text{-ML Mn/Co/Ni/Cu}$ according to the magnetic hysteresis loops of (a). In (b), the yellow shadow indicates the estimated critical thicknesses for the onset of induced perpendicular magnetization at 300 K. In (c), the gray shadow indicates the estimated critical thickness for the onset of AFM–FM exchange coupling (H_c enhancement) as well as an established long-range AFM ordering of $\text{Ni}_{50}\text{Mn}_{50}$ films at room temperature.

C. PMA triggered in NiMn-based AFM/Co/Ni films

To explore another possible approach for triggering PMA by using $\text{Ni}_{50}\text{Mn}_{50}$ -based AFM films, we applied a structurally compatible single-layered Mn film at the interface of the $\text{Ni}_{50}\text{Mn}_{50}$ and Co/Ni films. As presented in Fig. 6(a), PMA was successfully triggered in the $\text{Ni}_{50}\text{Mn}_{50}/1\text{-ML Mn/Co/Ni}$ films. Figures 6(a)–6(c) display the concurrently established PMA and H_c enhancement (long-range AFM ordering) of $\text{Ni}_{50}\text{Mn}_{50}/1\text{-ML Mn/Co/Ni}$ films when t_{NiMn} reached 9 ML; that is, the value close to the threshold for the onset of long-range AFM ordering of $\text{Ni}_{50}\text{Mn}_{50}$ films [Fig. 5(d)]. Thus, the finding of PMA in the $\text{Ni}_{50}\text{Mn}_{50}/1\text{-ML Mn/Co/Ni}$ films suggests that the incorporation of a 1-ML Mn film at the interface could critically change the exchange coupling orientation across the $\text{Ni}_{50}\text{Mn}_{50}$ and Co/Ni films. Because PMA in $\text{Ni}_{50}\text{Mn}_{50}/1\text{-ML Mn/Co/Ni}$ films occurs only when the $\text{Ni}_{50}\text{Mn}_{50}$ film reaches the AFM state ($t_{\text{NiMn}} \geq 9$ ML), the PMA is expected to be attributable to the exchange coupling from not only the magnetic moments of the 1-ML Mn film at the interface but also those AFM moments in the volume of the $\text{Ni}_{50}\text{Mn}_{50}$ film. To further examine the roles of the volume moments of the AFM films in triggering PMA, we measured the magnetic hysteresis loops of a series of Mn/1-ML $\text{Ni}_{50}\text{Mn}_{50}/\text{Co/Ni}$ films in which the stacking structure of the AFM film was inverse to the aforementioned

$\text{Ni}_{50}\text{Mn}_{50}/1\text{-ML Mn/Co/Ni}$ system. As shown in Fig. 7(a), stable PMA was also triggered when $t_{\text{Mn}} > 3$ ML, the threshold for an enhanced H_c value as well as established long-range AFM ordering of Mn films [Figs. 7(b) and 7(c)]. This result suggests that PMA can be supported by those Mn moments in the volume, even if 1-ML $\text{Ni}_{50}\text{Mn}_{50}$ with lower Mn moment density is applied as the interface layer.

Figure 8 summarizes the magnetic properties of a series of NiMn-based AFM/Co/Ni films with the AFM thickness fixed at 10 ML. For 10-ML $\text{Ni}_{50}\text{Mn}_{50}/\text{Co/Ni}$ film [Fig. 8(a)], PMA could not be triggered although the long-range AFM ordering of $\text{Ni}_{50}\text{Mn}_{50}$ films was established ($t_{\text{NiMn}} \geq 9$ ML); this may be attributable to an inadequate Mn moment density at the interface of the $\text{Ni}_{50}\text{Mn}_{50}$ film. Instead, PMA was induced when the Mn concentration was increased in full NiMn alloy films [Fig. 8(b)]. According to Figs. 8(a)–8(c), a higher value of perpendicular H_c is obtained when the Mn concentration is increased. Moreover, PMA can also be triggered by applying composite AFM films comprising Mn and $\text{Ni}_{50}\text{Mn}_{50}$ layers [Figs. 8(d) and 8(e)]. As shown in Fig. 8(f), which summarizes the H_c values of various perpendicularly magnetic 10-ML NiMn-based AFM/Co/Ni films, increasing the Mn concentration either at the interface or in the volume of the NiMn-based AFM films can promote the H_c value of perpendicular magnetization induced in an adjacent Co/Ni film. Thus, by probing the magnetic properties induced by

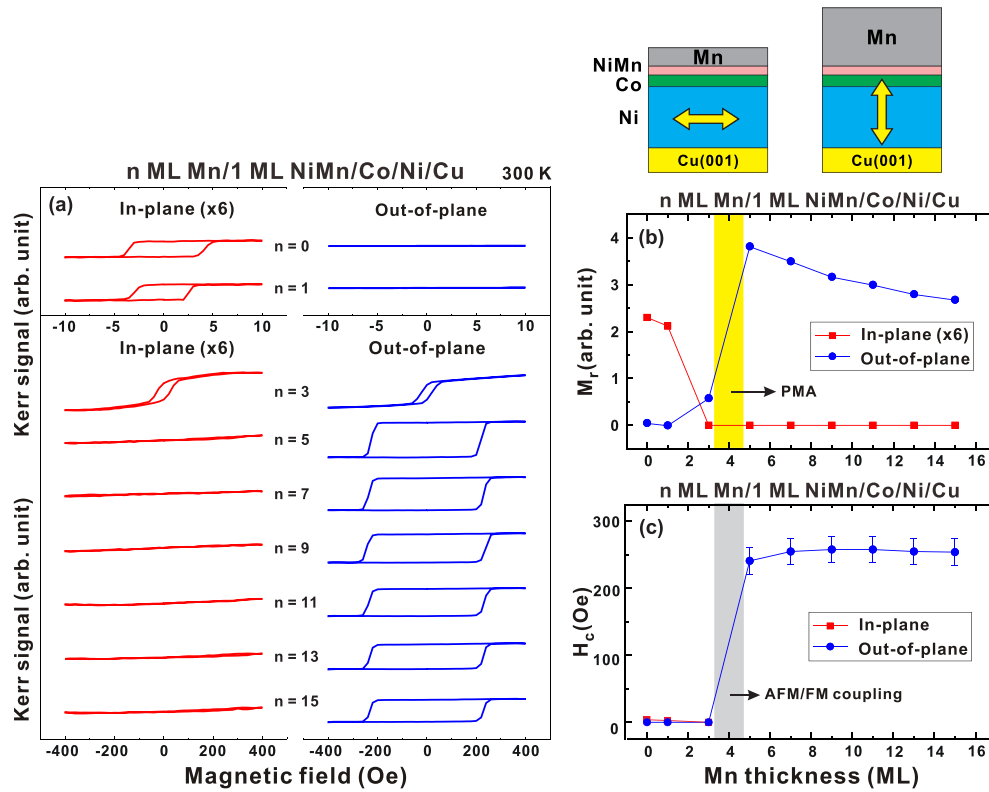


FIG. 7. Magnetic hysteresis loops of (a) 0–15-ML Mn/1-ML Ni₅₀Mn₅₀/Co/Ni/Cu. The measurements were performed at room temperature. (b) and (c): summarized M_r and H_c values of 0–15-ML Mn/1-ML Ni₅₀Mn₅₀/Co/Ni/Cu according to the magnetic hysteresis loops of (a). In (b), the yellow shadow indicates the estimated critical thicknesses for the onset of induced perpendicular magnetization at 300 K. In (c), the gray shadow indicates the estimated critical thickness for the onset of AFM-FM exchange coupling (H_c enhancement) as well as an established long-range AFM ordering of Mn films at room temperature.

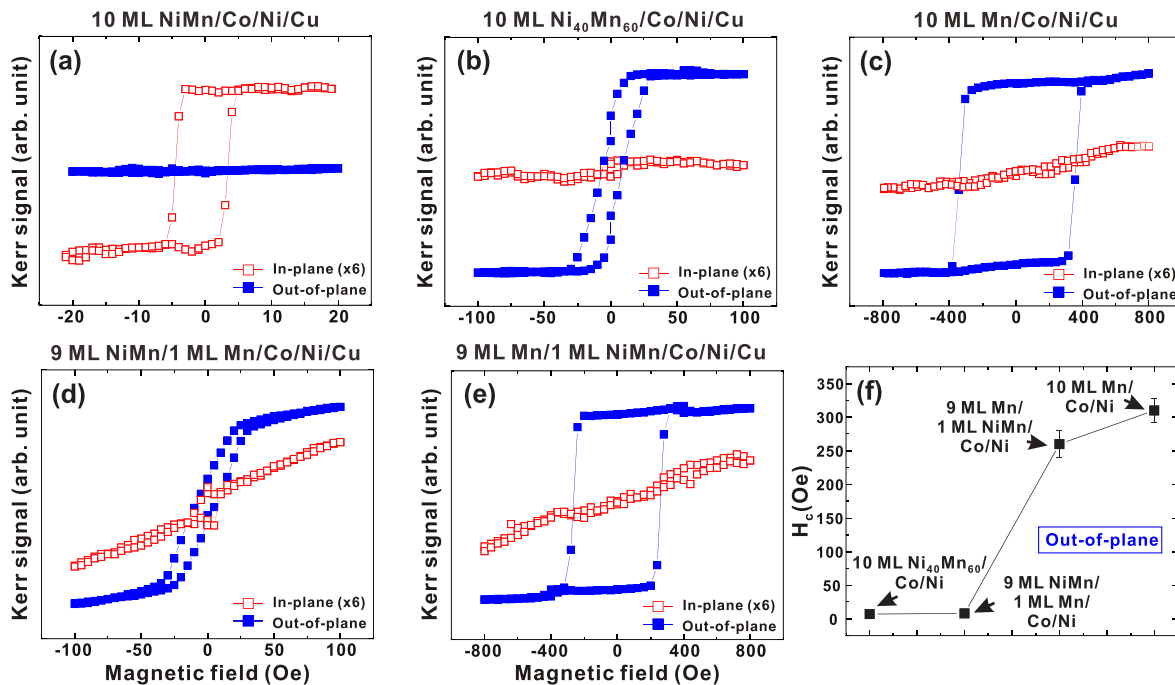


FIG. 8. In-plane and out-of-plane magnetic hysteresis loops of (a) 10-ML Ni₅₀Mn₅₀/Co/Ni/Cu, (b) 10-ML Ni₄₀Mn₆₀/Co/Ni/Cu, (c) 10-ML Mn/Co/Ni/Cu, (d) 9-ML Ni₅₀Mn₅₀/1-ML Mn/Co/Ni/Cu, and (e) 9-ML Mn/1-ML Ni₅₀Mn₅₀/Co/Ni/Cu. The measurements were performed at room temperature. (f) Summarized H_c values of various perpendicular magnetic films.

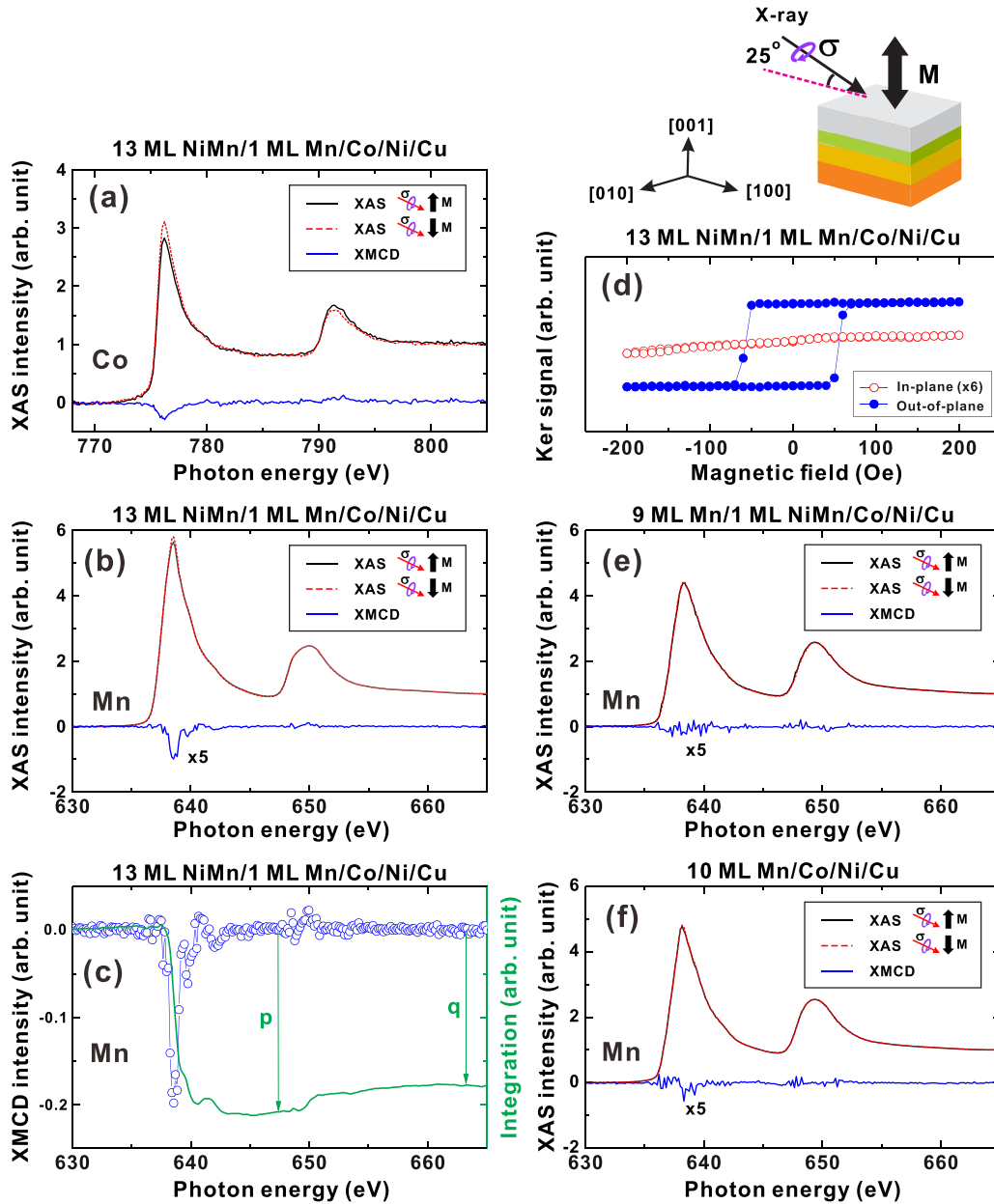


FIG. 9. (a) Co and (b) Mn $L_{3,2}$ edges XAS and corresponding XMCD curves of 13-ML $\text{Ni}_{50}\text{Mn}_{50}/1\text{-ML Mn/Co/Ni/Cu}$. (c) XMCD and integration curves of 13-ML $\text{Ni}_{50}\text{Mn}_{50}/1\text{-ML Mn/Co/Ni/Cu}$. The p and q values indicate the integration of the XMCD curve in the L_3 and $L_3 + L_2$ regions, respectively. (e) and (f): Mn $L_{3,2}$ edges XAS and XMCD curves of 9-ML Mn/1-ML $\text{Ni}_{50}\text{Mn}_{50}/\text{Co/Ni/Cu}$ and 10-ML Mn/Co/Ni/Cu, respectively. In each figure, σ and \mathbf{M} denote the photohelicity of incident x rays and the magnetization direction of the films, respectively.

NiMn-based AFM films with various combinations, we demonstrated that both interfacial and volume moments of the AFM film are crucial for triggering the PMA of adjacent FM films.

D. Interfacial uncompensated Mn moments of NiMn-based AFM/Co/Ni films

To further understand the role of the interfacial Mn moments on PMA induced in NiMn-based AFM/Co/Ni films, measurements of XMCD at Mn, Co, and Ni $L_{3,2}$ edges were performed. Figures 9(a)–9(c) display the selected Co and Mn XAS and XMCD curves of a perpendicularly magnetic

13-ML $\text{Ni}_{50}\text{Mn}_{50}/1\text{-ML Mn/Co/Ni}$ film [Fig. 9(d)] [38]. According to the sign of the observed XMCD asymmetry at L_3 edge, the Mn uncompensated moments coupled in parallel with the Co moments at the AFM-FM interface. Figure 9(c) displays the enlarged Mn XMCD and its integration curves. The p and q values given by the integration of the XMCD curve in the L_3 and $L_3 + L_2$ regions respectively indicate the sum of magnetic asymmetry in both regions. Assume a negligible magnetic dipole operator term in the spin sum rule [39,40], which is small for $3d$ metals [41]. Next, p and q values can be used to calculate the ratio of orbit to spin moments as follows: $m_{\text{orbit}}/m_{\text{spin}} = 2q/(9p - 6q)$ [42], thereby

obtaining information on crystalline anisotropy [25,43]. Accordingly, a high orbit-to-spin ratio of 0.42 for the interfacial Mn uncompensated moments was obtained.

According to Hund's rule, the Mn ion in pure $3d^5$ configuration is unable to contribute large orbit moments. Practically, however, finite values of Mn orbit moments and even sizable Mn-induced crystalline anisotropy have been observed in many Mn-based low dimensional heterosystems [7,9,44,45]. These behaviors could be attributed to the effects of orbital hybridization between the Mn atoms and other elements under the broken symmetry of crystal field [25,44,45]; in these cases, the Mn ions are no longer in pure $3d^5$ configuration. In the present investigated NiMn(Mn)/Co/Ni/Cu systems, the crystal field at the Mn/Co interface is also highly asymmetric; the d_{\perp} of Mn is reduced to about 1.74 \AA ($c/a \approx 0.96$) at interface compared to 1.88 \AA ($c/a \approx 1.04$) in volume [Figs. 4(b) and 4(c)]. Thus, as demonstrated in the Supplemental Material [46], hybridization between the interfacial Mn and Co orbitals along the out-of-plane direction could occur; this could therefore trigger the existence of out-of-plane orbit moments of the interfacial Mn atoms. However, because of an overlapping between the L_3 and L_2 edges in Mn XAS spectra which reduces the p value in the integration curve [Fig. 9(c)], the $m_{\text{orbit}}/m_{\text{spin}}$ ratio (0.42) of the interfacial Mn uncompensated moments extracted from the sum rule could be overestimated. In fact, the sum rule for the orbit moments involves the integration over the XMCD spectrum, i.e., the q value [42]. Thus, in the present work, an observation of the large q value according to Fig. 9(c) supports the presence of sizable out-of-plane orbit moments of the interfacial Mn uncompensated moments. Accordingly, current results suggest the formation of high-strength perpendicular interface crystalline anisotropy with regard to those Mn uncompensated moments at the AFM-FM interface of the perpendicularly magnetic 13-ML NiMn/1-ML Mn/Co/Ni film. For the 9-ML Mn/1-ML Ni₅₀Mn₅₀/Co/Ni and 10-ML Mn/Co/Ni films [Figs. 9(e) and 9(c)] that exhibit higher values of perpendicular H_c (260–300 Oe), however, the Mn XMCD signals were significantly reduced. Because of a similar condition of the AFM-FM interface between the 13-ML Ni₅₀Mn₅₀/1-ML Mn/Co/Ni and 10-ML Mn/Co/Ni films, a reduction in the uncompensated level of the interfacial Mn moments in the latter case was expected to be highly associated with the exchange coupling effects from the volume moments of the AFM Mn layer. This topic is discussed in a later section.

IV. DISCUSSION

A. Correlation between the uncompensated level of Mn moments and the strength of lateral exchange coupling in NiMn-based AFM films

Regarding the XMCD examination of the perpendicularly magnetic 13-ML Ni₅₀Mn₅₀/1-ML Mn/Co/Ni film [Figs. 9(a) and 9(b)], uncompensated Mn moments coupled in parallel to the magnetization of Co were detected. However, the Mn XMCD signal was significantly reduced for the perpendicularly magnetic Mn/Co/Ni film that exhibited a relatively large value of H_c and relatively strong PMA [Fig. 9(f)]. This accords observations of reductions in the Mn XMCD signal in exchange-coupled e-fct Mn/Co bilayers [47,48].

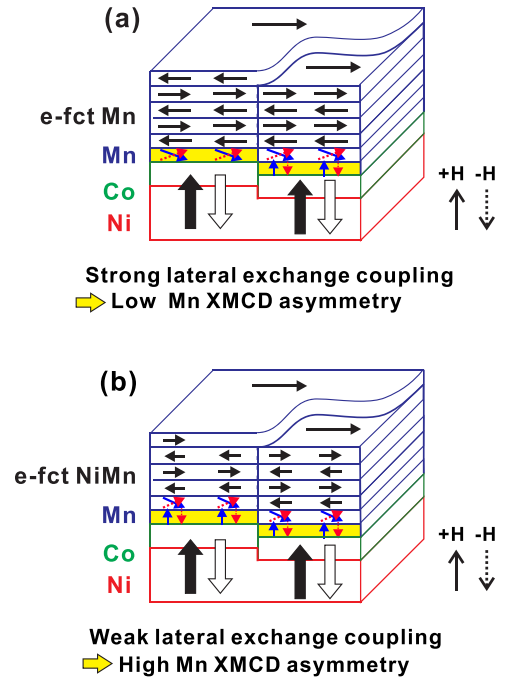


FIG. 10. Schematic illustrations of the spin structures in perpendicularly magnetic (a) Mn/Co/Ni and (b) Ni₅₀Mn₅₀/1-ML Mn/Co/Ni films. A single atomic step is used in both models for simulating a presence of interface roughness inherent from the grain boundary or substrate terrace. The bold black and white arrows indicate the magnetization direction of the Co/Ni films under positive and negative out-of-plane-oriented magnetic fields ($+H$ and $-H$), respectively. The blue (solid) and red (dashed) arrows in the yellow area indicate that the interfacial uncompensated Mn moments respectively switched under $+H$ and $-H$; these moments coupled noncollinearly with the volume moments of AFM films. In (a), the out-of-plane components of the interfacial Mn moments close to the surface step could be reduced through strong lateral exchange coupling from in-plane-oriented Mn moments on other Co steps. A similar effect could be reduced in (b) because the lateral exchange coupling from adjacent Ni₅₀Mn₅₀ moments was relatively weak.

By comparing fcc-like Mn films with various in-plane lattice strains, studies have demonstrated that a reduction in the Mn XMCD signal can be triggered by spin frustration across the same Mn interfacial layer induced by a hidden Co step inherent from the grain boundary or substrate terrace [49]. Moreover, such an effect is enlarged when the strength of the lateral exchange coupling of the Mn moments is enhanced. When considering the perpendicularly magnetic Mn/Co/Ni systems investigated in this study, the low XMCD signal of the Mn interfacial moments may also be attributable to a similar mechanism of lateral exchange coupling. As presented in Fig. 10(a), under the assumption of strong lateral exchange coupling of the volume Mn moments, the out-of-plane components of those interfacial Mn moments located close to the step edges could be considerably reduced by exchange coupling effects from the in-plane-oriented moments of the Mn films grown on another Co step, which could result in a serious reduction of the Mn XMCD signal. By contrast, under the assumption that Ni₅₀Mn₅₀ exhibits relatively weak lateral exchange coupling [Fig. 10(b)],

the ordering of the layered-like AFM structure mainly follows the magnetization direction of the Co step underneath, and the out-of-plane uncompensated Mn moments at the interface are less affected by the in-plane-oriented moments of the Ni₅₀Mn₅₀ film grown on another Co step. These out-of-plane uncompensated Mn moments close to the interface were observed through XMCD. Thus, the current XMCD results indicate that the strength of the lateral exchange coupling of the e-fct Mn film can be substantially higher than that of an e-fct Ni₅₀Mn₅₀ film; our thickness-dependent MOKE measurements offer further support for this finding. According to the results presented in Figs. 6 and 7, the threshold thickness for the onset of long-range AFM ordering as well as the induction of PMA in Mn/1-ML Ni₅₀Mn₅₀/Co/Ni films (≈ 4 ML) is considerably lower than in Ni₅₀Mn₅₀/1-ML Mn/Co/Ni (≈ 9 ML), meaning that the Mn film exhibits stronger lateral exchange coupling than does Ni₅₀Mn₅₀ according to finite size effects [50]. In addition, stronger lateral exchange coupling in e-fct Mn, relative to that in e-fct Ni₅₀Mn₅₀, can also be understood in view of microscopic spin configuration. According to previous SP-STM works [14,15,22], e-fct Mn and e-fct Ni₅₀Mn₅₀ films exhibit similar in-plane spin orientations but different distributions of AFM moment density [Figs. 1(a) and 1(b)]. Regarding e-fct Mn, a distribution of in-plane-oriented spin moments in a full single layer was detected [14,15]. Regarding the e-fct Ni₅₀Mn₅₀ film, however, the magnetic moments were mainly contributed by the Mn atoms (only half a layer) [22]. Thus, a lower density of in-plane moments in e-fct Ni₅₀Mn₅₀, compared with those in e-fct Mn films, may result in weaker lateral exchange coupling in AFM layers.

B. Roles of the interfacial and volume moments of NiMn-based AFM films on induced PMA

According to current results, e-fct Ni₅₀Mn₅₀ films alone cannot induce PMA in adjacent Co/Ni films. PMA was induced when a single-layered Mn film was inserted between the Ni₅₀Mn₅₀ and Co/Ni layers, suggesting that the level of Mn moment density at the interface of a NiMn-based AFM film is crucial for triggering PMA in neighboring Co/Ni films. According to an observation of a high orbit/spin ratio of Mn uncompensated moments in 13-ML Ni₅₀Mn₅₀/1-ML Mn/Co/Ni film [Fig. 9(c)], out-of-plane oriented Mn uncompensated moments with strong perpendicular interface crystalline anisotropy were detected. We speculate that these interfacial Mn moments are responsible for the stabilization of the PMA of the Co/Ni layers underneath when they couple with those in-plane-oriented Mn moments in the volume of e-fct Ni₅₀Mn₅₀ or Mn films [14,15,22]. However, the preceding discussion prompted another crucial question: why is PMA enhanced when the lateral exchange coupling of the volume moments of the NiMn-based AFM film is increased? As mentioned, enhancement of lateral exchange coupling, caused by increasing the Mn moment density in the volume

of the NiMn-based AFM film, could reduce the perpendicular components of those Mn uncompensated moments close to the edge of the Co step [Fig. 10(a)]. However, supported by the perpendicular interface crystalline anisotropy of the interfacial Mn moments, strengthening the lateral exchange coupling can create numerous domain walls at the AFM-FM interface. In an exchange-coupled AFM/FM bilayer with established AFM ordering, the domain-wall activated processes, caused by the pinning effects from the AFM layer, can typically result in enhanced H_c values [3,25,49]. In the present study, we expected that a similar pinning mechanism could also lead to enhanced H_c in perpendicularly magnetic 10-ML Mn/Co/Ni (≈ 300 Oe) compared with that in 13-ML Ni₅₀Mn₅₀/1-ML Mn/Co/Ni films (≈ 60 Oe) [Fig. 8(f)]. We have provided a comprehensive picture revealing the roles of interfacial and volume moments of the NiMn-based AFM films in inducing PMA in neighboring FM films, thereby answering the question of why PMA can be promoted by increasing the Mn moment density in either the interface or volume of the NiMn-based AFM films. Moreover, our results indicate the establishment of noncollinear exchange coupling in perpendicularly magnetic NiMn-based AFM/Co/Ni films. Our findings are essential for the development of the field of antiferromagnet-induced PMA and frontier perpendicular magnetic recording technology comprising AFM films with in-plane-oriented spin structures.

V. CONCLUSION

We comprehensively examined the effects of triggering PMA through the application of a series of NiMn-based AFM films with in-plane spin orientations. We demonstrated that PMA can be successfully triggered by increasing the Mn concentration in full NiMn alloy films or by applying Ni₅₀Mn₅₀/Mn (Mn/Ni₅₀Mn₅₀) heterostructures. Our detailed analysis determined that establishing perpendicular interface crystalline anisotropy of the interfacial uncompensated Mn moments and inducing strengthened lateral exchange coupling to the volume AFM moments are two essential criteria for a NiMn-based AFM film to trigger PMA in a neighboring FM film. Our findings not only clarify the mechanism for triggering PMA through AFM films with an in-plane-oriented AFM spin structure but also demonstrate a possible approach of interface/volume magnetic engineering to promote the control of antiferromagnet-induced PMA. These findings could inspire the application of PMA in next-generation perpendicular spintronic devices consisting of AFM films with in-plane-oriented spin structures.

ACKNOWLEDGMENT

This work was partly supported by the Ministry of Science and Technology, Taiwan (Grant No. MOST 109-2112-M-018-001).

[1] W. H. Meiklejohn and C. P. Bean, *Phys. Rev.* **102**, 1413 (1956).

[2] W. H. Meiklejohn and C. P. Bean, *Phys. Rev.* **105**, 904 (1957).

[3] J. Nogués and I. K. Schuller, *J. Magn. Magn. Mater.* **192**, 203 (1999).

[4] S. D. Bader, *Rev. Mod. Phys.* **78**, 1 (2006).

- [5] S. Mao, Z. Gao, H. Xi, P. Kolbo, M. Plumer, L. Wang, A. Goyal, I. Jin, J. Chen, C. Hou, R. M. White, and E. Murdock, *IEEE Trans. Magn.* **38**, 26 (2002).
- [6] B. Y. Wang, N. Y. Jih, W. C. Lin, C. H. Chuang, P. J. Hsu, C. W. Peng, Y. C. Yeh, Y. L. Chan, D. H. Wei, W. C. Chiang, and M.-T. Lin, *Phys. Rev. B* **83**, 104417 (2011).
- [7] B.-Y. Wang, J.-Y. Hong, K.-H.-O. Yang, Y.-L. Chan, D.-H. Wei, H.-J. Lin, and M.-T. Lin, *Phys. Rev. Lett.* **110**, 117203 (2013).
- [8] B.-Y. Wang, M.-S. Tsai, C.-W. Huang, C.-W. Shih, C.-J. Chen, K. Lin, J.-J. Li, N.-Y. Jih, C.-I. Lu, T.-H. Chuang, and D.-H. Wei, *Phys. Rev. B* **96**, 094416 (2017).
- [9] B.-Y. Wang, P.-H. Lin, M.-S. Tsai, C.-W. Shih, M.-J. Lee, C.-W. Huang, N.-Y. Jih, P.-Y. Cheng, and D.-H. Wei, *Phys. Rev. B* **92**, 214435 (2015).
- [10] W. Kuch, L. I. Chelaru, F. Offi, J. Wang, M. Kotsugi, and J. Kirschner, *Phys. Rev. Lett.* **92**, 017201 (2004).
- [11] J. S. Kouvel and J. S. Kasper, *J. Phys. Chem. Solids* **24**, 529 (1963).
- [12] H. Umebayashi and Y. Ishikawa, *J. Phys. Soc. Jpn.* **21**, 1281 (1966).
- [13] M. Ekholm and I. A. Abrikosov, *Phys. Rev. B* **84**, 104423 (2011).
- [14] P.-J. Hsu, C.-I. Lu, Y.-H. Chu, B.-Y. Wang, C.-B. Wu, L.-J. Chen, S.-S. Wong, and M.-T. Lin, *Phys. Rev. B* **85**, 174434 (2012).
- [15] C. B. Wu, J. Song, and W. Kuch, *Appl. Phys. Lett.* **101**, 012404 (2012).
- [16] M. F. Toney, M. G. Samant, T. Lin, and D. Mauri, *Appl. Phys. Lett.* **81**, 4565 (2002).
- [17] P. M. Oppeneer, H.-C. Mertins, D. Abramssohn, A. Gaupp, W. Gudat, J. Kuneš, and C. M. Schneider, *Phys. Rev. B* **67**, 052401 (2003).
- [18] J. S. Kasper and J. S. Kouvel, *J. Phys. Chem. Solids* **11**, 231 (1959).
- [19] E. Krén, E. Nagy, I. Nagy, L. Pál, and P. Szabó, *J. Phys. Chem. Solids* **29**, 101 (1968).
- [20] C. Tieg, W. Kuch, S. G. Wang, and J. Kirschner, *Phys. Rev. B* **74**, 094420 (2006).
- [21] M. Reinhardt, J. Seifert, M. Busch, and H. Winter, *Phys. Rev. B* **81**, 134433 (2010).
- [22] C. L. Gao, A. Ernst, A. Winkelmann, J. Henk, W. Wulfhchel, P. Bruno, and J. Kirschner, *Phys. Rev. Lett.* **100**, 237203 (2008).
- [23] J. Shen, J. Giergiel, and J. Kirschner, *Phys. Rev. B* **52**, 8454 (1995).
- [24] W. C. Lin, C. C. Kuo, C. L. Chiu, and M. T. Lin, *Surf. Sci.* **478**, 9 (2001).
- [25] J. Stöhr and H. C. Siegmann, *Magnetism: From Fundamentals to Nanoscale Dynamics* (Springer, Berlin, 2006).
- [26] J. Stöhr, Y. Wu, B. D. Hermsmeier, M. G. Samant, G. R. Harp, S. Koranda, D. Dunham, and B. P. Tonner, *Science* **259**, 658 (1993).
- [27] C. M. Schneider and G. Schönhense, *Rep. Prog. Phys.* **65**, R1785 (2002).
- [28] D.-H. Wei, Y.-L. Chan, and Y.-J. Hsu, *J. Electron Spectrosc. Relat. Phenom.* **185**, 429 (2012).
- [29] A. Scholl, J. Stöhr, J. Lüning, J. W. Seo, J. Fompeyrine, H. Siegart, J. P. Locquet, F. Nolting, S. Anders, E. E. Fullerton, M. R. Scheinfein, and H. A. Padmore, *Science* **287**, 1014 (2000).
- [30] F. Nolting, A. Scholl, J. Stöhr, J. W. Seo, J. Fompeyrine, H. Siegart, J. P. Locquet, S. Anders, J. Lüning, E. E. Fullerton, M. F. Toney, M. R. Scheinfein, and H. A. Padmore, *Nature (London)* **405**, 767 (2000).
- [31] H. Ohldag, A. Scholl, F. Nolting, S. Anders, F. U. Hillebrecht, and J. Stöhr, *Phys. Rev. Lett.* **86**, 2878 (2001).
- [32] W. Kim, E. Jin, J. Wu, J. Park, E. Arenholz, A. Scholl, C. Hwang, and Z. Q. Qiu, *Phys. Rev. B* **81**, 174416 (2010).
- [33] W. J. Antel Jr., F. Perjeru, and G. R. Harp, *Phys. Rev. Lett.* **83**, 1439 (1999).
- [34] F. Offi, W. Kuch, and J. Kirschner, *Phys. Rev. B* **66**, 064419 (2002).
- [35] C. Won, Y. Z. Wu, H. W. Zhao, A. Scholl, A. Doran, W. Kim, T. L. Owens, X. F. Jin, and Z. Q. Qiu, *Phys. Rev. B* **71**, 024406 (2005).
- [36] K. Lenz, S. Zander, and W. Kuch, *Phys. Rev. Lett.* **98**, 237201 (2007).
- [37] Q. Li, J.-H. Liang, Y.-M. Luo, Z. Ding, T. Gu, Z. Hu, C.-Y. Hua, H.-J. Lin, T.-W. Pi, S.-P. Kang, C. Won, and Y.-Z. Wu, *Sci. Rep.* **6**, 22355 (2016).
- [38] The XMCD signal from the FM Ni layer is interfered by the Ni signal from NiMn. Therefore, the results of Ni are not discussed here.
- [39] B. T. Thole, P. Carra, F. Sette, and G. van der Laan, *Phys. Rev. Lett.* **68**, 1943 (1992).
- [40] P. Carra, B. T. Thole, M. Altarelli, and X. Wang, *Phys. Rev. Lett.* **70**, 694 (1993).
- [41] R. Wu, D. Wang, and A. J. Freeman, *Phys. Rev. Lett.* **71**, 3581 (1993).
- [42] C. T. Chen, Y. U. Idzerda, H. J. Lin, N. V. Smith, G. Meigs, E. Chaban, G. H. Ho, E. Pellegrin, and F. Sette, *Phys. Rev. Lett.* **75**, 152 (1995).
- [43] P. Bruno, *Phys. Rev. B* **39**, 865 (1989).
- [44] K. W. Edmonds, G. van der Laan, N. R. S. Farley, E. Arenholz, R. P. Campion, C. T. Foxon, and B. L. Gallagher, *Phys. Rev. B* **77**, 113205 (2008).
- [45] H. Ohldag, V. Solinus, F. U. Hillebrecht, J. B. Goedkoop, M. Finazzi, F. Matsukura, and H. Ohno, *Appl. Phys. Lett.* **76**, 2928 (2000).
- [46] See Supplemental Material at <http://link.aps.org/supplemental/10.1103/PhysRevB.104.024424> for information on the sum rule analysis of the Co element.
- [47] M. Caminale, R. Moroni, P. Torelli, W. C. Lin, M. Canepa, L. Mattera, and F. Bisio, *Phys. Rev. Lett.* **112**, 037201 (2014).
- [48] W. L. O'Brien and B. P. Tonner, *Phys. Rev. B* **50**, 2963 (1994).
- [49] B.-Y. Wang, J.-Y. Hong, N.-Y. Jih, K.-H. Ou Yang, L.-R. Chen, H.-J. Lin, Y.-L. Chan, D.-H. Wei, and M.-T. Lin, *Phys. Rev. B* **90**, 224424 (2014).
- [50] T. Ambrose and C. L. Chien, *Phys. Rev. Lett.* **76**, 1743 (1996).